Simultaneous Optimization of Nuclear–Electronic Orbitals

Aodong Liu,[†] Mathew Chow,[‡] Andrew Wildman,[†] Michael J. Frisch,[¶] Sharon Hammes-Schiffer,*,[‡] and Xiaosong Li*,[†],§

†Department of Chemistry, University of Washington, Seattle, WA 98195, USA

‡Department of Chemistry, Yale University, New Haven, CT 06520, USA

¶Gaussian Inc., 340 Quinnipiac St, Bldg 40, Wallingford, CT 06492, USA

§Pacific Northwest National Laboratory, Richland, WA 99354, USA

E-mail: sharon.hammes-schiffer@yale.edu; xsli@uw.edu

Abstract

Accurate modeling of important nuclear quantum effects, such as nuclear delocalization, zero-point energy, and tunneling, as well as non-Born-Oppenheimer effects, requires treatment of both nuclei and electrons quantum mechanically. The nuclear–electronic orbital (NEO) method provides an elegant framework to treat specified nuclei, typically protons, on the same level as the electrons. In conventional electronic structure theory, finding a converged ground state can be a computationally demanding task; converging NEO wavefunctions, due to their coupled electronic and nuclear nature, is even more demanding. Herein, we present an efficient simultaneous optimization method that uses the direct inversion in the iterative subspace method to simultaneously converge wavefunctions for both the electrons and quantum nuclei. Benchmark studies show that the simultaneous optimization method can significantly reduce the computational cost compared to the conventional stepwise method for optimizing NEO wavefunctions for multicomponent systems.

1 Introduction

In conventional electronic structure calculations, the Born-Oppenheimer approximation is invoked to separate electronic and nuclear degrees of freedom. Often the nuclei are assumed to move classically on the adiabatic potential energy surface, which can be obtained by solving the electronic time-independent Schrödinger equation at each nuclear configuration. However, nuclear quantum effects, as well as non-Born-Oppenheimer effects in some cases, play an important role in many chemical processes, such as proton-coupled electron transfer, ¹⁻⁴ photoinduced proton transfer, ⁵⁻⁹ hydrogen tunneling, ^{10,11} and hydrogen-bonding interactions. ¹² Many methods have been developed to account for the nuclear quantum effects within or beyond the Born-Oppenheimer approximation, such as the Ehrenfest dynamics, ¹³⁻¹⁶ surface hopping, ¹⁷⁻¹⁹ multiconfigurational time-dependent Hartree (MCTDH), ²⁰⁻²³ multiple spawning, ²⁴⁻²⁷ ring polymer path integral, ^{28,29} and Gaussian wave packet dynamics ^{30,31} methods. In many cases, however, the computational expense and scaling impose limitations on the system size, and the more efficient methods are often lacking some of the important nonadiabatic or nuclear quantum effects.

The nuclear–electronic orbital (NEO) method ^{32–38} provides a robust and computationally efficient framework that treats specified nuclei, typically protons, quantum mechanically on the same level as the electrons. In the NEO approach, both electronic and nuclear molecular orbitals are expressed as linear combinations of Gaussian-type orbitals, and the energy is minimized variationally with respect to the mixed nuclear–electronic wavefunction. The main advantage of the NEO approach is that it intrinsically incorporates nuclear quantum effects and non-Born-Oppenheimer effects in the electronic–nuclear structure calculation, giving rise to a computational framework capable of simulating nonadiabatic reaction dynamics. ^{16,39–41}

All NEO calculations start with a procedure to converge the NEO orbitals to a stationary wavefunction. However, as the complexity (*i.e.*, the numbers of electrons and quantum nuclei) of the NEO system increases, efficiently solving for the nuclear-electronic wavefunction becomes a computationally challenging task. In this work, we introduce a simultaneous

optimization algorithm to self-consistently solve the NEO-Roothaan-Hall equations. A simultaneous direct inversion in the iterative subspace approach is developed to improve the convergence stability and speed, as supported by benchmark studies.

2 Method

2.1 NEO Hamiltonian and Hartree–Fock Wavefunction

In the NEO framework, specified nuclei, typically protons, are treated quantum mechanically. The system can be divided into three parts: N^e electrons, N^p quantum nuclei, and N^c classical nuclei. This leads to the following NEO Hamiltonian, expressed in atomic units:

$$\hat{H}_{NEO} = -\sum_{i}^{N^{e}} \frac{1}{2} \nabla_{i}^{2} + \sum_{i}^{N^{e}} \sum_{j>i}^{N^{e}} \frac{1}{|\mathbf{r}_{i} - \mathbf{r}_{j}|} - \sum_{i}^{N^{e}} \sum_{A}^{N^{c}} \frac{Z_{A}}{|\mathbf{r}_{i} - \mathbf{R}_{A}|}$$

$$-\sum_{I}^{N^{p}} \frac{1}{2M_{I}} \nabla_{I}^{2} + \sum_{I}^{N^{p}} \sum_{J>I}^{N^{p}} \frac{Z_{I}Z_{J}}{|\mathbf{r}_{I} - \mathbf{r}_{J}|} + \sum_{I}^{N^{p}} \sum_{A}^{N^{c}} \frac{Z_{A}Z_{I}}{|\mathbf{r}_{I} - \mathbf{R}_{A}|}$$

$$-\sum_{i}^{N^{e}} \sum_{I}^{N^{p}} \frac{Z_{I}}{|\mathbf{r}_{i} - \mathbf{r}_{I}|} + \sum_{A}^{N^{c}} \sum_{B>A}^{N^{c}} \frac{Z_{A}Z_{B}}{|\mathbf{R}_{A} - \mathbf{R}_{B}|}$$
(1)

where $\{i, j, ...\}$, $\{I, J, ...\}$, and $\{A, B, ...\}$ are indices for electrons, quantum nuclei, and classical nuclei, respectively. The nuclear masses and charges, respectively, are denoted by M and Z. \mathbf{R} and \mathbf{r} are the positions of the classical and quantum particles, respectively. For the remainder of this paper, the quantum nuclei will be assumed to be protons.

A key objective of the NEO approach is to solve the NEO time-independent Schrödinger equation for a fixed classical nuclear configuration $\{\mathbf{R}_A\}$:

$$H_{\text{NEO}}\Psi(\boldsymbol{x}^e, \boldsymbol{x}^p; \{\mathbf{R}_A\}) = E_{\text{NEO}}\Psi(\boldsymbol{x}^e, \boldsymbol{x}^p; \{\mathbf{R}_A\}), \tag{2}$$

where x^e and x^p are the collective spatial and spin coordinates of the electrons and quantum protons, respectively. The simplest NEO wavefunction ansatz is the Hartree-Fock wave-

function,³² in which the total wavefunction is expressed as a product of the electronic and protonic Slater determinants:

$$\Psi(\boldsymbol{x}^e, \boldsymbol{x}^p) = \Phi^e(\boldsymbol{x}^e)\Phi^p(\boldsymbol{x}^p). \tag{3}$$

where Φ^e and Φ^p are determinants consisting of electronic and nuclear orbitals, respectively.

In practice, the electronic and nuclear spatial orbitals are expanded in Gaussian-type basis functions. In the NEO-Hartree-Fock (NEO-HF) approach, the energy is optimized variationally with the self-consistent-field (SCF) procedure, leading to the following NEO Hartree-Fock-Roothaan equations:

$$\mathbf{F}^e \mathbf{C}^e = \mathbf{S}^e \mathbf{C}^e \boldsymbol{\epsilon}^e \tag{4}$$

$$\mathbf{F}^p \mathbf{C}^p = \mathbf{S}^p \mathbf{C}^p \boldsymbol{\epsilon}^p, \tag{5}$$

where \mathbf{F}^e , \mathbf{S}^e , \mathbf{C}^e , and $\boldsymbol{\epsilon}^e$ are the electronic Fock matrix, overlap matrix, coefficient matrix, and orbital energies, respectively, and the quantum nuclear matrices are defined analogously.

Equation (4) and Equation (5) are coupled through the Coulombic interaction between the electrons and quantum nuclei, which can be readily seen from the construction of the Fock matrix for each subsystem:

$$\mathbf{F}^{e}(\mathbf{P}^{e}, \mathbf{P}^{p}) = \mathbf{H}_{core}^{e} + \mathbf{J}^{ee}(\mathbf{P}^{e}) + \mathbf{K}^{ee}(\mathbf{P}^{e}) + \mathbf{J}^{ep}(\mathbf{P}^{e}, \mathbf{P}^{p})$$
(6)

$$\mathbf{F}^{p}(\mathbf{P}^{p}, \mathbf{P}^{e}) = \mathbf{H}_{\text{core}}^{p} + \mathbf{J}^{pp}(\mathbf{P}^{p}) + \mathbf{K}^{pp}(\mathbf{P}^{p}) + \mathbf{J}^{pe}(\mathbf{P}^{p}, \mathbf{P}^{e}). \tag{7}$$

where \mathbf{P}^e and \mathbf{P}^p are the electronic and quantum nuclear density matrices, respectively. $\mathbf{H}_{\text{core}}^{e(p)}$ is the one-body core Hamiltonian matrix for the electrons (quantum nuclei). $\mathbf{J}^{ee(pp)}$ and $\mathbf{K}^{ee(pp)}$ are the Coulomb and exchange matrices, respectively, for the electrons (quantum nuclei). \mathbf{J}^{ep} and \mathbf{J}^{pe} account for the Coulombic interaction between the electrons and

quantum nuclei, and their matrix elements can be computed as

$$\mathbf{J}_{\mu^p\nu^p}^{pe} = -\sum_{\lambda^e\kappa^e}^{K^e} \mathbf{P}_{\lambda^e\kappa^e}^e (\mu^p \nu^p | \kappa^e \lambda^e)$$
 (8)

$$\mathbf{J}_{\mu^e \nu^e}^{ep} = -\sum_{\lambda^p \kappa^p}^{K^p} \mathbf{P}_{\lambda^p \kappa^p}^p (\mu^e \nu^e | \kappa^p \lambda^p), \tag{9}$$

where $K^{e(p)}$ is the number of basis functions for the electronic (quantum nuclear) subsystem, and $\{\mu^e, \nu^e, \sigma^e, \lambda^e, ...\}$ and $\{\mu^p, \nu^p, \sigma^p, \lambda^p, ...\}$ represent the electronic and quantum nuclear basis functions, respectively.

2.2 Direct Inversion in the Iterative Subspace (DIIS)

Direct Inversion in the Iterative Subspace (DIIS) is a least-squares minimization method that can accelerate the SCF convergence. ^{42,43} In DIIS, an improved Fock matrix \mathbf{F}' can be expressed as a linear combination of the previous Fock matrices \mathbf{F}_i :

$$\mathbf{F}' = \sum_{i=1}^{n} c_i \mathbf{F}_i, \qquad \sum_{i=1}^{n} c_i = 1, \tag{10}$$

where n is the iteration number in the SCF procedure.

The DIIS approach seeks to minimize the error associated with the improved Fock matrix, \mathbf{F}' :

$$\mathbf{e}' = \sum_{i=1}^{n} c_i \mathbf{e}_i \tag{11}$$

where \mathbf{e}_i quantifies the error associated with \mathbf{F}_i . Applying the least-squares minimization

procedure to Eq. (11) gives rise to the following equation represented in matrix form:

$$\begin{pmatrix}
B_{11} & B_{12} & B_{13} & \dots & B_{1n} & 1 \\
B_{21} & B_{22} & B_{23} & \dots & B_{2n} & 1 \\
B_{31} & B_{32} & B_{33} & \dots & B_{3n} & 1 \\
\vdots & \vdots & \vdots & \ddots & \vdots & \vdots \\
B_{n1} & B_{n2} & B_{n3} & \dots & B_{nn} & 1 \\
1 & 1 & 1 & \dots & 1 & 0
\end{pmatrix}
\cdot
\begin{pmatrix}
c_1 \\
c_2 \\
c_3 \\
\vdots \\
c_n \\
\lambda
\end{pmatrix} =
\begin{pmatrix}
0 \\
0 \\
\vdots \\
0 \\
1
\end{pmatrix}$$
(12)

where $B_{ij} = \langle \mathbf{e}_i | \mathbf{e}_j \rangle$. Solving Eq. (12) yields a set of coefficients that minimize the error and can then be used to construct an improved Fock matrix using Eq. (10). The diagonalization of \mathbf{F}' leads to a new set of orbitals used to construct the density matrix to start the next iteration.

The effectiveness of DHS relies on the choice of an error vector that can properly quantify the error associated with each Fock matrix. At convergence of the SCF procedure, the density matrix must commute with the Fock matrix. It is therefore possible to define an error vector at iteration i as 42,43

$$\mathbf{e}_i = \mathbf{S}\mathbf{P}_i\mathbf{F}_i - \mathbf{F}_i\mathbf{P}_i\mathbf{S},\tag{13}$$

which is known as the commutator DIIS approach. Other types of error vectors include conjugate gradient, ⁴⁴ energy, ^{45,46} and quasi-Newton-Raphson step. ⁴⁷ In this work, we will focus on generalizing Eq. (13) to the NEO framework in the simultaneous optimization algorithm for both electronic and nuclear orbitals.

2.3 Simultaneous Optimization Algorithm

In the NEO-SCF procedure, two Fock matrices, \mathbf{F}^e and \mathbf{F}^p , need to be optimized to convergence. The conventional protocol in the literature³⁸ is the stepwise optimization algorithm, where either the electronic or quantum nuclear SCF equations are fully converged while

freezing the density of the other subsystem, proceeding in an alternating fashion until both equations (Eq. (4) and Eq. (5)) are converged. A schematic of this algorithm is shown in Fig. 1(A). Within each electronic/protonic SCF, DIIS can be used to accelerate the convergence. Although this protocol can usually arrive at a converged NEO wavefunction, the number of Fock matrix formations dramatically increases when the system of interest becomes large, and the computational cost can become very demanding.

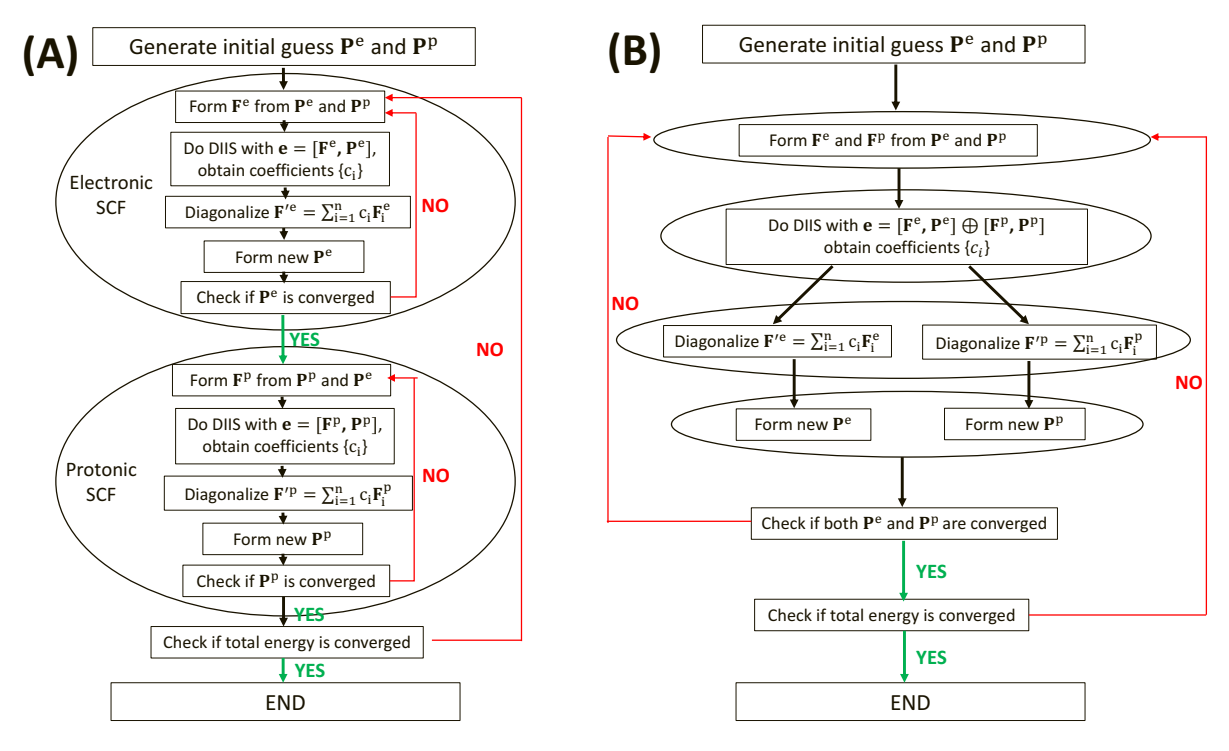


Figure 1. (A) Schematic illustration of the stepwise NEO-SCF algorithm. (B) Schematic illustration of the simultaneous NEO-SCF algorithm.

Alternatively, all variational parameters in the whole system can be simultaneously optimized, as exemplified by the previous success of simultaneous optimization for the electronic wavefunction and polarizable continuum model, ⁴⁸ and for the electronic wavefunction and molecular geometry. ⁴⁹ Herein, we propose a simultaneous optimization scheme to converge NEO wavefunctions, where both electronic and quantum nuclear Roothaan equations (Eq. (4) and Eq. (5)) are simultaneously solved in each SCF iteration. A schematic of this algorithm is shown in Fig. 1(B). We apply the DIIS method to accelerate the convergence

of both the electronic and the protonic wavefunctions by constructing the error vector to be the sum of the subsystem error vectors:

$$B_{ij} = \langle \mathbf{e}_i^e | \mathbf{e}_i^e \rangle + \langle \mathbf{e}_i^p | \mathbf{e}_i^p \rangle, \tag{14}$$

where

$$\mathbf{e}_i^e = \mathbf{S}^e \mathbf{P}_i^e \mathbf{F}_i^e - \mathbf{F}_i^e \mathbf{P}_i^e \mathbf{S}^e, \qquad \mathbf{e}_i^p = \mathbf{S}^p \mathbf{P}_i^p \mathbf{F}_i^p - \mathbf{F}_i^p \mathbf{P}_i^p \mathbf{S}^p.$$

By solving Eq. (12), a set of least-squares coefficients can be obtained and used to construct improved electronic and protonic Fock matrices via extrapolation/interpolation:

$$\mathbf{F}^{\prime e} = \sum_{i=1}^{n} c_i \mathbf{F}_i^e, \qquad \mathbf{F}^{\prime p} = \sum_{i=1}^{n} c_i \mathbf{F}_i^p$$
(15)

In this manner, the coefficients are optimized with respect to both electronic and protonic degrees of freedom. At each SCF iteration, improved electronic and protonic Fock matrices are diagonalized to give rise to updated electronic and protonic orbitals, thus achieving the simultaneous optimization.

3 Results and Discussion

Both the stepwise and the simultaneous optimization algorithms are implemented for the NEO-HF method in the development version of the Gaussian software. 50 The benchmark studies presented in this work will include the SCF convergence profiles for both energy and density using both stepwise and simultaneous optimization methods with various electronic and protonic basis sets. The NEO wavefunction is considered fully converged when the root-mean-square electronic/protonic density difference is below 10^{-8} a.u. and the energy difference is below 10^{-10} Hartree between two consecutive steps. In the following benchmark calculations, up to 10 previous Fock/density matrices are used in the DHS extrapolation/interpolation. The initial wavefunction guess occupies the tightest protonic basis function for

each quantum proton and uses this charge distribution to do the Harris guess⁵¹ for the electronic orbitals. When the system consists of multiple protons, they are placed in a high-spin protonic configuration.

In Fig. 2, we present the results obtained from NEO-SCF calculations on the cis-Zundel isomer of the protonated water tetramer. All nine hydrogens in this system are treated quantum mechanically with the PB5d protonic basis set. 52 The cc-pVTZ correlation consistent basis set 53 is used for the electronic subsystem. For this test case, the simultaneous optimization algorithm shows a much faster convergence, meeting all three convergence thresholds within 174 SCF iterations. In contrast, the conventional stepwise approach requires 90 electronic and 570 protonic iterations to reach convergence. Figure 2(A) shows that both methods converge the energy monotonically, although the simultaneous approach exhibits a much faster convergence. Figure 2(B) and Figure 2(C) show the trend for the root-mean-square density difference (RMS Δ) for \mathbf{P}^e and \mathbf{P}^p , computed as RMS $\Delta \mathbf{P} = \frac{1}{K} \sqrt{\sum_{\mu\nu} |P_{n,\mu\nu} - P_{n-1,\mu\nu}|^2}$, where K is the number of basis functions. These figures show that the stepwise algorithm introduces long segments of 'waiting time' when one subsystem is waiting for the other to fully converge, leading to a slower overall convergence. The big 'jump' in the RMS ΔP convergence profile occurs when the subsystem experiences a sudden change in interaction potential between the two subsystems at the start of a new iteration. This jump is a result of the decoupled optimization in the stepwise optimization. In contrast, the simultaneous DIIS algorithm takes into account errors associated with both electronic and protonic wavefunctions, and therefore it is able to find the optimal pathway to converge the coupled subsystems smoothly toward the minimum. In Fig. 3, we zoom in on the energy and RMS ΔP trend for the simultaneous DIIS optimization algorithm. This figure shows that both the electronic and protonic densities are converging at the same time. The trend for the two densities exhibits the same behavior, as both subsystems share the same set of coefficients to extrapolate the next Fock matrix using Eq. (15).

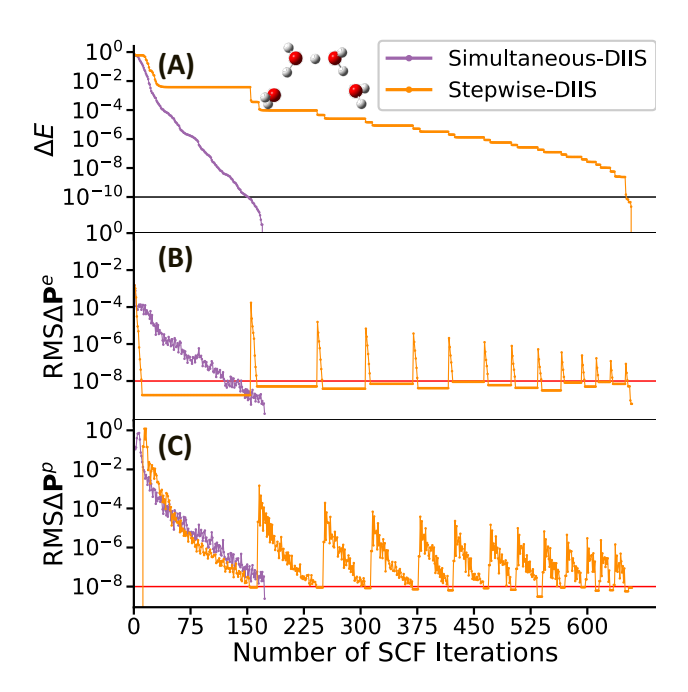


Figure 2. NEO-HF calculations performed on the cis-Zundel isomer of the protonated water tetramer using either the stepwise or simultaneous optimization DIIS algorithm with the cc-pVTZ/PB5d electronic/nuclear basis sets. (A) Energy difference between two consecutive steps. (B) Root-mean-square electronic density difference between two consecutive steps, RMS ΔP^e . (C) Root-mean-square protonic density difference between two consecutive steps, RMS ΔP^p . The black/red horizontal line represents the energy/density convergence threshold.

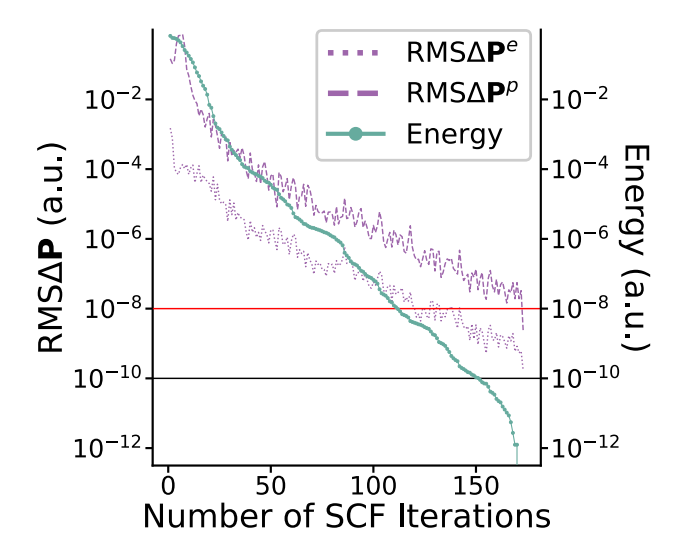


Figure 3. NEO-HF calculations performed on the cis-Zundel isomer of the protonated water tetramer using the simultaneous optimization DIIS algorithm with the cc-pVTZ/PB5d electronic/protonic basis sets. The energy and the electronic and protonic RMS $\Delta \mathbf{P}$ decrease together for the simultaneous optimization algorithm with DIIS. The black/red horizontal line represents the energy/density convergence threshold.

We then compare the computational costs of both algorithms. The Fock matrix formation in the NEO-SCF procedure is the most expensive step, as it requires the contraction of 4-index integrals and formally scales as N^4 , where N is the number of basis functions. In the stepwise algorithm, each SCF iteration only includes either the electronic or the protonic Fock matrix formation, whereas in the simultaneous algorithm, each SCF iteration includes formation of both the electronic and protonic Fock matrices. Therefore, the computational cost for a NEO-SCF calculation using the direct algorithm (integrals computed on-the-fly) based on Eq. (6) and Eq. (7) can be formally calculated as:

$$f(N^e, N^p) = a_e(N^e)^4 + a_p(N^p)^4 + (a_e + a_p)(N^e)^2(N^p)^2,$$
(16)

where the prefactors a_e and a_p are the numbers of electronic and protonic Fock matrix formations, respectively. The last term in Eq. (16) accounts for the computational cost from Eq. (8) and Eq. (9). We use Eq. (16) as the unbiased metric to analyze and benchmark the performance of both algorithms.

To provide a more systematic analysis of the basis set and system size dependence of the simultaneous DIIS algorithm, we first consider small test systems with one or two quantum protons using correlation consistent electronic basis sets 53 and various protonic basis sets developed by Yu et al. 52 The results are shown in Fig. 4. The simultaneous DIIS optimization can dramatically reduce the cost of NEO-SCF calculations, exhibiting an average of $\sim 60\%$ savings compared to the traditional stepwise algorithm for the systems shown in Fig. 4. The excellent performance of the simultaneous optimization method also holds for larger test cases. In Fig. 5, we performed NEO-SCF calculations on four isomers of the protonated water tetramer complex, using the def2-TZVP 54 electronic basis set and the PB4d 52 protonic basis set. The results consistently show that the simultaneous DIIS algorithm can reduce the computational cost by an average of 56% compared to the stepwise algorithm.

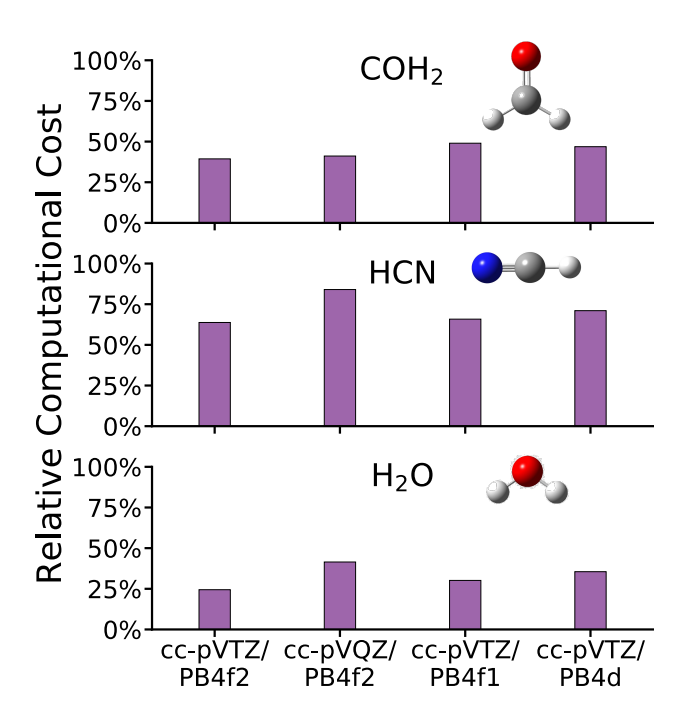


Figure 4. Relative computational cost of a NEO-HF calculation for three small molecules. The x axis describes the basis set used for electrons/quantum protons in each calculation. The relative cost is evaluated as $\frac{f_{\text{simultaneous}}}{f_{\text{stepwise}}}$, where the f's are calculated using Eq. (16) for the simultaneous and stepwise DIIS algorithms.

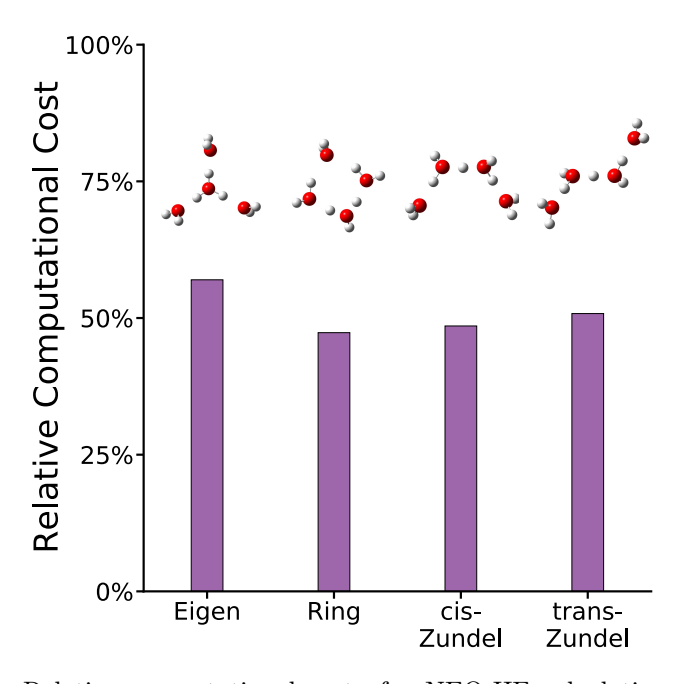


Figure 5. Relative computational cost of a NEO-HF calculation for isomers of the protonated water tetramers. The relative cost is evaluated as $\frac{f_{\text{simultaneous}}}{f_{\text{stepwise}}}$, where the f's are calculated using Eq. (16) for the simultaneous and stepwise algorithms.

In Fig. 6, we show the relative computational cost of the simultaneous and stepwise algorithms for optimizing the NEO-HF wavefunctions of a protonated water tetramer using different basis sets. For a given electronic basis set, as the number of protonic basis functions increases, the simultaneous optimization algorithm exhibits an overall trend of increased computational saving compared to the stepwise algorithm. For a fixed protonic basis set, however, increasing the size of the electronic basis set decreases this computational savings. This trend is observed because the reduction in the number of nuclear optimization steps by the simultaneous optimization algorithm is much greater than that for the electronic optimization step. As the number of nuclear basis functions increases, the computational cost of the nuclear Fock build becomes more dominant. As a result, the simultaneous optimization algorithm exhibits better computational performance compared to the stepwise approach. On the other hand, since the number of electronic SCF iterations is comparable between the two algorithms, the simultaneous method can only marginally improve the convergence speed when the electronic Fock build is the dominant computational cost. In other words, a_e is similar for the two algorithms, but a_p is smaller for the simultaneous optimization algorithm. Thus, as the number of electronic basis functions dominates, the two algorithms approach the same cost, whereas as the number of protonic basis functions dominates, the simultaneous optimization will have lower cost.

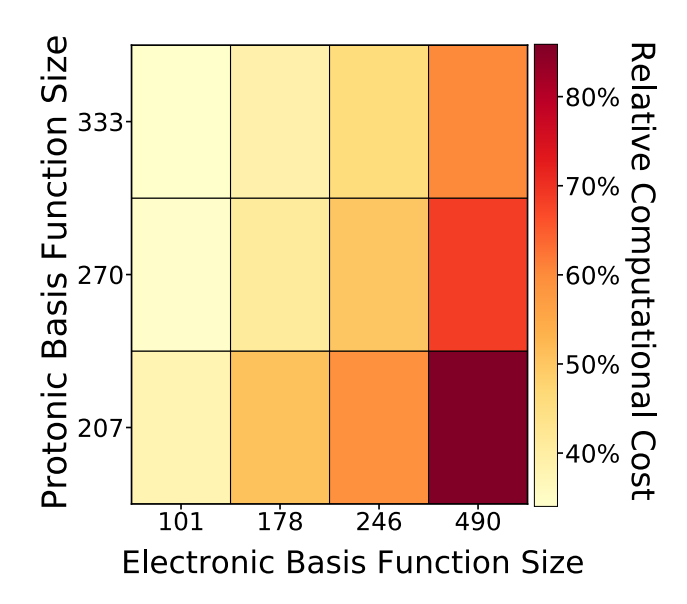


Figure 6. Relative computational cost of a NEO-HF calculation for isomers of the protonated water tetramer as a function of basis set size. The relative cost is evaluated as $\frac{f_{\text{simultaneous}}}{f_{\text{stepwise}}}$, where the f's are calculated using Eq. (16) for the simultaneous and stepwise algorithms.

4 Conclusions

In this paper, we present an efficient algorithm for NEO-SCF calculations that utilizes DIIS to simultaneously converge the electronic and protonic orbitals. This simultaneous optimization algorithm uses an error vector that takes into account both the electronic and protonic errors at each step. Benchmark calculations show that the simultaneous optimization can significantly reduce the computational cost needed to converge the NEO wavefunction, compared to the conventional stepwise method. As the main savings in computational cost arises from the reduction in the number of nuclear SCF iterations, the simultaneous optimization algorithm becomes more efficient as the number of nuclear basis functions increases.

Supporting Information

The supporting information includes: molecular structures; comparison of NEO and conventional electronic SCF calculations.

Acknowledgement

The development of quantum dynamics for studies of proton transfer was supported by IDREAM (Interfacial Dynamics in Radioactive Environments and Materials), an Energy Frontier Research Center funded by the U.S. Department of Energy (DOE), Office of Science, Basic Energy Sciences (BES). The development of nuclear-electronic orbital time-dependent density functional theory methods is supported by the National Science Foundation (Grant No. CHE-1954348 to SHS and CHE-2154346 to XL). The development of the Chronus Quantum computational software is supported by the Office of Advanced Cyberinfrastructure, National Science Foundation (Grant No. OAC-2103717). Computations were facilitated through the use of advanced computational, storage, and networking infrastructure provided by the Hyak supercomputer system at the University of Washington, funded by the Student Technology Fee.

References

- Huynh, M. H. V.; Meyer, T. J. Proton-Coupled Electron Transfer. Chem. Rev. 2007, 107, 5004–5064.
- (2) Hammes-Schiffer, S.; Stuchebrukhov, A. A. Theory of Coupled Electron and Proton Transfer Reactions. *Chem. Rev.* **2010**, *110*, 6939–6960.
- (3) Weinberg, D. R.; Gagliardi, C. J.; Hull, J. F.; Murphy, C. F.; Kent, C. A.; Westlake, B. C.; Paul, A.; Ess, D. H.; McCafferty, D. G.; Meyer, T. J. Proton-Coupled Electron Transfer. *Chem. Rev.* **2012**, *112*, 4016–4093.
- (4) Hammes-Schiffer, S. Proton-Coupled Electron Transfer: Moving Together and Charging Forward. J. Am. Chem. Soc. **2015**, 137, 8860–8871.
- (5) Chou, P.-T.; Solntsev, K. M. Photoinduced Proton Transfer in Chemistry and Biology. J. Phys. Chem. B 2015, 119, 2089.
- (6) Pines, E.; Pines, D. In Ultrafast Hydrogen Bonding Dynamics and Proton Transfer Prosesses in the Condensed Phase; Elsaesser, T., Bakker, H. J., Eds.; Springer Netherlands: Dordrecht, 2002; pp 155–184.
- (7) Nibbering, E. T. J.; Fidder, H.; Pines, E. Ultrafast Chemistry: Using Time-Resolved Vibrational Spectroscopy for Interrogation of Structural Dynamics. Annu. Rev. Phys. Chem. 2005, 56, 337–367.
- (8) Domcke, W.; Sobolewski, A. L. Chemistry. Unraveling the Molecular Mechanisms of Photoacidity. *Science* **2003**, *302*, 1693–1694.
- (9) Agmon, N. Elementary Steps in Excited-State Proton Transfer. J. Phys. Chem. A 2005, 109, 13–35.
- (10) Cha, Y.; Murray, C. J.; Klinman, J. P. Hydrogen Tunneling in Enzyme Reactions. Science 1989, 243, 1325–1330.

- (11) Borgis, D.; Hynes, J. T. Dynamical Theory of Proton Tunneling Transfer Rates in Solution: General Formulation. *Chem. Phys.* **1993**, *170*, 315–346.
- (12) Ceriotti, M.; Fang, W.; Kusalik, P. G.; McKenzie, R. H.; Michaelides, A.; Morales, M. A.; Markland, T. E. Nuclear Quantum Effects in Water and Aqueous Systems: Experiment, Theory, and Current Challenges. J. Am. Chem. Soc. 2016, 116, 7529–7550.
- (13) Li, X.; Tully, J. C.; Schlegel, H. B.; Frisch, M. J. Ab Initio Ehrenfest Dynamics. J. Chem. Phys. 2005, 123, 084106.
- (14) Isborn, C. M.; Li, X.; Tully, J. C. TDDFT Ehrenfest Dynamics: Collisions between Atomic Oxygen and Graphite Clusters. *J. Chem. Phys.* **2007**, *126*, 134307.
- (15) Ding, F.; Goings, J. J.; Liu, H.; Lingerfelt, D. B.; Li, X. Ab Initio Two-Component Ehrenfest Dynamics. J. Chem. Phys. 2015, 143, 114105.
- (16) Zhao, L.; Wildman, A.; Tao, Z.; Schneider, P.; Hammes-Schiffer, S.; Li, X. Nuclear–Electronic Orbital Ehrenfest dynamics. *J. Chem. Phys.* **2020**, *153*, 224111.
- (17) Tully, J. C. Trajectory Surface Hopping Approach to Nonadiabatic Molecular Collisions: The Reaction of H+ with D₂. J. Chem. Phys. **1971**, 55, 562.
- (18) Tully, J. C. Molecular Dynamics with Electronic Transitions. J. Chem. Phys. 1990, 93, 1061.
- (19) Tully, J. C. Perspective: Nonadiabatic Dynamic Theory. J. Chem. Phys. 2012, 137, 22A301.
- (20) Beck, M. H.; Jäckle, A.; Worth, G. A.; Meyer, H.-D. The Multiconfiguration Time-dependent Hartree (MCTDH) Method: A Highly Efficient Algorithm for Propagating Wavepackets. *Phys. Rep.* 2000, 324, 1–105.

- (21) Wang, H.; Thoss, M. Multilayer Formulation of the Multiconfiguration Time-Dependent Hartree Theory. J. Chem. Phys. 2003, 119, 1289.
- (22) Worth, G. A.; Meyer, H.-D.; Köppel, H.; Cederbaum, L. S.; Burghardt, I. Using the MCTDH Wavepacket Propagation Method to Describe Multimode Non-Adiabatic Dynamics. Int. Rev. Phys. Chem. 2008, 27, 569–606.
- (23) Manthe, U. A Multilayer Multiconfigurational Time-Eependent Hartree Approach for Quantum Dynamics on General Potential Energy Surfaces. J. Chem. Phys. 2008, 128, 164116.
- (24) Martinez, T. J.; Ben-Nun, M.; Levine, R. D. Multi-Electronic-State Molecular Dynamics: A Wave Function Approach with Applications. J. Phys. Chem. 1996, 100, 7884–7895.
- (25) Ben-Nun, M.; Quenneville, J.; Martínez, T. J. A Multilayer Multiconfigurational Time-Eependent Hartree Approach for Quantum Dynamics on General Potential Energy Surfaces. J. Phys. Chem. A 2000, 104, 5161–5175.
- (26) Tao, H.; Levine, B. G.; Martínez, T. J. Ab Initio Multiple Spawning Dynamics Using Multi-State Second-Order Perturbation Theory. J. Phys. Chem. A 2009, 113, 13656–13662.
- (27) Curchod, B. F. E.; Martínez, T. J. Ab Initio Nonadiabatic Quantum Molecular Dynamics. *Chem. Rev.* **2018**, *118*, 3305–3336.
- (28) Craig, I. R.; Manolopoulos, D. E. Chemical Reaction Rates From Ring Polymer Molecular Dynamics. J. Chem. Phys. 2005, 122, 084106.
- (29) Habershon, S.; Manolopoulos, D. E.; Markland, T. E.; Miller, T. F., 3rd Ring-polymer Molecular Dynamics: Quantum Effects in Chemical Dynamics from Classical Trajectories in an Extended Phase Space. Annu. Rev. Phys. Chem. 2013, 64, 387–413.

- (30) Huber, D.; Heller, E. J. Generalized Gaussian Wave Packet Dynamics. *J. Chem. Phys.* **1987**, *87*, 5302.
- (31) Heller, E. J. Guided Gaussian Wave Packets. Acc. Chem. Res. 2006, 39, 127–134.
- (32) Webb, S. P.; Iordanov, T.; Hammes-Schiffer, S. Multiconfigurational Nuclear-Electronic Orbital Approach: Incorporation of Nuclear Quantum Effects in Electronic Structure Calculations. J. Chem. Phys. 2002, 117, 4106–4118.
- (33) Yang, Y.; Brorsen, K. R.; Culpitt, T.; Pak, M. V.; Hammes-Schiffer, S. Development of a Practical Multicomponent Density Functional for Electron-Proton Correlation to Produce Accurate Proton Densities. J. Chem. Phys. 2017, 147, 114113.
- (34) Yang, Y.; Culpitt, T.; Hammes-Schiffer, S. Multicomponent Time-Dependent Density Functional Theory: Proton and Electron Excitation Energies. J. Phys. Chem. Lett. 2018, 9, 1765–1770.
- (35) Culpitt, T.; Yang, Y.; Pavošević, F.; Tao, Z.; Hammes-Schiffer, S. Enhancing the Applicability of Multicomponent Time-Dependent Density Functional Theory. *J. Chem. Phys.* **2019**, *150*, 201101.
- (36) Pavošević, F.; Culpitt, T.; Hammes-Schiffer, S. Multicomponent Coupled Cluster Singles and Doubles Theory within the Nuclear-Electronic Orbital Framework. *J. Chem. Theory Comput.* **2019**, *15*, 338–347.
- (37) Pavošević, F.; Tao, Z.; Culpitt, T.; Zhao, L.; Li, X.; Hammes-Schiffer, S. Frequency and Time Domain Nuclear–Electronic Orbital Equation-of-Motion Coupled Cluster Methods: Combination Bands and Electronic–Protonic Double Excitations. *J. Phys. Chem. Lett.* **2020**, *11*, 6435–6442.
- (38) Pavošević, F.; Culpitt, T.; Hammes-Schiffer, S. Multicomponent Quantum Chemistry:

- Integrating Electronic and Nuclear Quantum Effects via the Nuclear-Electronic Orbital Method. Chem. Rev. 2020, 120, 4222–4253.
- (39) Zhao, L.; Tao, Z.; Pavošević, F.; Wildman, A.; Hammes-Schiffer, S.; Li, X. Real-Time Time-Dependent Nuclear-Electronic Orbital Approach: Dynamics Beyond the Born-Oppenheimer Approximation. J. Phys. Chem. Lett. 2020, 11, 4052–4058.
- (40) Zhao, L.; Wildman, A.; Pavošević, F.; Tully, J. C.; Hammes-Schiffer, S.; Li, X. Excited State Intramolecular Proton Transfer with Nuclear-Electronic Orbital Ehrenfest Dynamics. J. Phys. Chem. Lett. 2021, 12, 3497–3502.
- (41) Wildman, A.; Tao, Z.; Zhao, L.; Hammes-Schiffer, S.; Li, X. Solvated Nuclear–Electronic Orbital Structure and Dynamics. J. Chem. Theory Comput. 2022, 18, 1340–1346.
- (42) Pulay, P. Convergence Acceleration of Iterative Sequences. the Case of Scf Iteration. *Chem. Phys. Lett.* **1980**, *73*, 393–398.
- (43) Pulay, P. Improved SCF Convergence Acceleration. J. Comput. Chem. 1982, 3, 556–560.
- (44) Li, X.; Millam, J. M.; Scuseria, G. E.; Frisch, M. J.; Schlegel, H. B. Density Matrix Search Using Direct Inversion in the Iterative Subspace as a Linear Scaling Alternative to Diagonalization in Electronic Structure Calculations. J. Chem. Phys. 2003, 119, 7651.
- (45) Kudin, K. N.; Scuseria, G. E.; Cances, E. A Black-box Self-consistent Field Convergence Algorithm: One Step Closer. *J. Chem. Phys.* **2002**, *116*, 8255–8261.
- (46) Li, X.; Frisch, M. J. Energy-Represented Direct Inversion in the Iterative Subspace within a Hybrid Geometry Optimization Method. *J. Chem. Theory Comput.* **2006**, *2*, 835–839.

- (47) Goings, J. J.; Ding, F.; Li, X. Self-Consistent Field Using Direct Inversion in Iterative Subspace Method and Quasi-Newton Vectors. *Adv. Quantum Chem.* **2014**, *68*, 77–86.
- (48) Lipparini, F.; Scalmani, G.; Mennucci, B.; Frisch, M. J. Self-Consistent Field and Polarizable Continuum Model: A New Strategy of Solution for the Coupled Equations. J. Chem. Theory Comput. 2011, 7, 610–617.
- (49) Moss, C. L.; Li, X. First Order Simultaneous Optimization of Molecular Geometry and Electronic Wave Function. *J. Chem. Phys.* **2008**, *129*, 114102.
- (50) Frisch, M. J.; Trucks, G. W.; Schlegel, H. B.; Scuseria, G. E.; Robb, M. A.; Cheeseman, J. R.; Scalmani, G.; Barone, V.; Petersson, G. A.; Nakatsuji, H. et al. *Gaussian Development Version Revision J.19*. Gaussian Inc., Wallingford CT 2020.
- (51) Harris, J. Simplified Method For Calculating the Energy of Weakly Interacting Fragments. *Phys. Rev. B Condens. Matter* **1985**, *31*, 1770–1779.
- (52) Yu, Q.; Pavošević, F.; Hammes-Schiffer, S. Development of Nuclear Basis Sets for Multicomponent Quantum Chemistry Methods. J. Chem. Phys. **2020**, 152, 244123.
- (53) Dunning, T. H. Gaussian Basis Sets for Use in Correlated Molecular Calculations. I. The Atoms Boron Through Neon and Hydrogen. J. Chem. Phys. 1989, 90, 1007–1023.
- (54) Weigend, F.; Ahlrichs, R. Balanced Basis Sets of Split Valence, Triple Zeta Valence and Quadruple Zeta Valence Quality for H to Rn: Design and Assessment of Accuracy. Phys. Chem. Chem. Phys. 2005, 7, 3297–3305.

TOC Graphic

